ESTIMATION OF THE DRAG COEFFICIENT OF MINE IMITATOR IN LONGITUDINAL AIR FLOW USING NUMERICAL METHODS

Algimantas Fedaravičius[1], Vaclovas Jonevičius[2], Sigitas Kilikevičius[3], Linas Paukštaitis[4], Povilas Šaulys [5]

[1, 3] *Kaunas University of Technology, Kęstučio g. 27, LT-44312 Kaunas, Lithuania*
[2] *Vilnius Gediminas Technical University, Plytinės g. 27, LT-10105 Vilnius, Lithuania*
[4] *Kaunas University of Technology, Donelaičio g. 20, LT-44239 Kaunas, Lithuania*
[5] *Kaunas Technical College, Tvirtovės g. 35, LT-50155 Kaunas, Lithuania*
E-mails: [1]algimantas.fedaravicius@ktu.lt (corresponding author); [2]vaclovas.jonevicius@vgtu.lt;
[3]sigitas.kilikevicius@ktu.lt; [4]linas.paukstaitis@ktu.lt; [5]povilas.saulys@ktu.lt

Abstract. One of the most important measures to reduce the cost of preparing mortar units is the use of mortar shooting trainers operating according to the 'shell in shell' principle that best meets the needs of military forces. When increasing the efficiency of using equipment for mortar shooting training and seeking to reduce their production costs, further research on external ballistics is strictly necessary in order to improve the structural parameters of mine imitators. With the help of finite element modelling techniques, this article investigates air flow over mortar mine imitators. In order to achieve the aim, a package of Mechanical Desktop Software was used for creating a dimensional model of mine imitator the model of which was imported into *ANSYS CFX* and a finite element numerical model was generated. Considering the literary sources of experimental studies, SST turbulence model generating the results closest to those of experimental research was selected. After modelling, air drag force influencing mine imitator and the drag coefficient at different air flow speed were established.

Keywords: mortar trainer, mine imitator, air flow, drag coefficient.

1. Introduction

The Armed Forces of developed countries are widely using trainers for training artillery specialists.

Presently, specialists from the Institute of Defence Technologies, Kaunas University of Technology; Kaunas Technical College and Vilnius Gediminas Technical University are dealing with the problem of firing 60 mm and 120 mm mortar trainers, which is extremely urgent to the Armed Forces of Lithuania (Fedaravičius *et al.* 2007, 2008a, b, 2009a, b).

The trainer consists of a sabot the external surface of which, in principal, repeats the contour of a combat mine. The inside is installed with a barrel with an infixed charge (Fig. 1). Mine imitators ('warheads') are inserted into a muzzle with the main powder charge while the rear part of the muzzle has several small holes intended for the distribution of the gas flow of the main powder charge. To imitate an explosion, 'the warhead' is filled with smoke powder and while falling into the ground it should explode in a way imitating the explosion of a mine. The 60 mm mortar trainer has four charges and 120 mm mortar trainer has five charges consisting of a 'warhead' and muzzle with respective amounts of powder that ensure firing ranges to the scale of 1/10 (Puoti *et al.* 2009; Fedaravičius *et al.* 2004, 2008a, b, 2009a).

Fig. 2 presents the operating scheme of the trainer. It shows separate phases of the trainer in operation: the insertion of the sabot and mine imitator into the barrel of the mortar (a); upon hitting the capsule of the main charge against the braking device at the bottom of the mortar barrel, the explosion of the main charge occurs (b), the energy of gas flow via the main barrel of the muzzle and ancillary holes is distributed in such a way that it rejects the sabot of the mine on a distance of 5÷25 m from the fire position of the mortar (d); 'the warhead' is in the range necessary to hit the target (c). Where 'the warhead' falls into the surface of the ground, the detonator goes off and initiates the explosion of the imitative smoke powder charge (Fedaravičius *et al.* 2005).

When speaking about the resistance of the bodies crossed by airflow, it is possible to state that the resistance of solid bodies over flown by the fluid is one of the
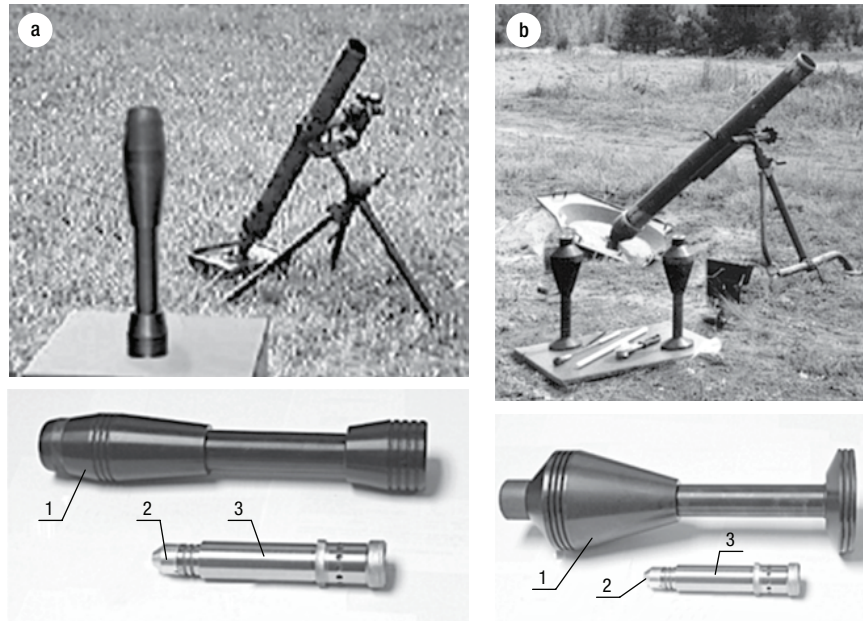
Fig. 1. The composition of a mortar shooting trainer: a – 60 mm mortar shooting trainer;
b – 120 mm mortar shooting trainer; 1 – sabot; 2 – mine imitator ('warhead'); 3 – muzzle
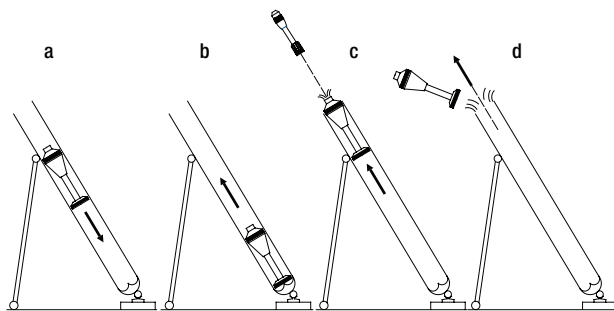

Fig. 2. An operating scheme of the trainer: a – sabot with
mine imitator inlet into the barrel of the mortar;
b – explosion of the main charge; c – traffic of the sabot and
mine imitator ('warhead') within the mortar barrel and its
environment; d – the falling phase of the sabot

main problems. The main task related to this problem is to identify drag forces that appear at the moment when the bodies are over flown. A solid body (mine imitator) moving in the fluid is influenced by drag force, thus, in order to overcome it, another force is necessary. The body in a moving fluid resists the flow with the same force.

2. Turbulent Models

One of the most difficult tasks of air flow turbulence modelling is to ensure accurate simulation results. A number of turbulence models are created; some of them are more accurate when speeds are high, the other are meant for modelling the boundary layer. Therefore, it is important to choose a turbulence model that allows making the most accurate comparison with experimental data (Lee *et al.* 2005).

Turbulence is a complex process, due to the fact it is mainly three dimensional, unsteady and consists of many scales. Turbulence occurs when inertia forces in the fluid become significant compared to viscous forces. Navier–Stokes equations describe both laminar and turbulent flows. However, turbulent flows at realistic Reynolds numbers span a large range of turbulent length and time scales. Therefore, CFD codes introduce turbulence models. Most turbulence models are statistical turbulence models.

2.1. RANS Equations

In this study, turbulence models seek to solve a modified set of transport equations by introducing averaged and fluctuating components. Substituting the averaged quantities into original transport equations results in the Reynolds averaged equations given below. The bar is dropped for averaged quantities, except for the products of fluctuating quantities:

$$\frac{\partial p}{\partial t} + \nabla \cdot (\rho U) = 0; \tag{1}$$

$$\frac{\partial \rho U}{\partial t} + \nabla \cdot (\rho U \cdot U) = -\nabla p + \nabla \cdot (\tau - \rho \overline{uu}) + S_M, \tag{2}$$

where: ρ – density; U – velocity; p – static (thermodynamic) pressure; τ – molecular stress tensor; $\rho \overline{uu}$ – Reynolds stresses; S_M – momentum source.

2.2. Eddy Viscosity Turbulence Models

The eddy viscosity hypothesis assumes that Reynolds stresses can be related to mean velocity gradients and eddy (turbulent) viscosity by the gradient diffusion hypothesis in a manner analogous to the relationship be-

tween stress and strain tensors in laminar Newtonian flow:

$$-\rho\,\overline{uu} = \mu_t\left(\nabla U + \left(\nabla U\right)^T\right) - \frac{2}{3}\delta_{ij}\left(\rho k + \mu_t \nabla U\right), \quad (3)$$

where: μ_t – eddy viscosity or turbulent viscosity; T – temperature; k – turbulence kinetic energy; ε – turbulence eddy dissipation.

The k–ε model assumes that turbulence viscosity is linked to turbulence kinetic energy and dissipation via relation:

$$\mu_t = C_\mu \rho \frac{k^2}{\varepsilon}, \quad (4)$$

where: C_μ – constant equal to 0.09 (*ANSYS CFX*).

The values of k and ε come directly from differential transport equations:

$$\frac{\partial\left(\rho k\right)}{\delta t} + \nabla\left(\rho U k\right) = \nabla\left(\left(\mu + \frac{\mu_t}{\sigma_k}\right)\nabla k\right) + P_k + P_{kb} - \rho\varepsilon; \quad (5)$$

$$\frac{\partial\left(\rho\varepsilon\right)}{\delta t} + \nabla\left(\rho U\varepsilon\right) = \nabla\left(\left(\mu + \frac{\mu_t}{\sigma_\varepsilon}\right)\nabla\varepsilon\right) +$$

$$\frac{\varepsilon}{k}\left(C_{\varepsilon1}\left(P_k + P_{\varepsilon b}\right) - C_{\varepsilon2}\rho\varepsilon\right), \quad (6)$$

where: $C_{\varepsilon1}$, $C_{\varepsilon2}$, σ_k and σ_ε – constants 1.44, 1.92 and 1.3 respectively (*ANSYS CFX... 2006*); P_k – turbulence production due to viscous forces.

2.3. k–ω Models

One of the advantages of k–ω formulation is near wall treatment for low-Reynolds number computations, which is therefore more accurate and robust then k–ε. The k–ω model assumes that turbulence viscosity is linked to turbulence kinetic energy and turbulent frequency via relation:

$$\mu_t = \rho\frac{k}{\omega}. \quad (7)$$

It solves two transport equations, one for turbulent kinetic energy k and one for turbulent frequency ω:

k equation:

$$\frac{\partial\left(\rho k\right)}{\delta t} + \nabla\left(\rho U k\right) =$$

$$\nabla\left(\left(\mu + \frac{\mu_t}{\sigma_k}\right)\nabla k\right) + P_k + P_{kb} - \beta'\rho k\omega; \quad (8)$$

ω equation:

$$\frac{\partial\left(\rho\omega\right)}{\delta t} + \nabla\left(\rho U\omega\right) = \nabla\left(\left(\mu + \frac{\mu_t}{\sigma_\omega}\right)\nabla\omega\right) +$$

$$\alpha\frac{\omega}{k}P_k + P_{\omega b} - \beta\rho\omega^2. \quad (9)$$

The constants of the model are given by:

$\beta' = 0.09$; $\alpha = 5/9$; $\beta = 0.075$; $\sigma_k = 2$; $\sigma_\omega = 2$.

2.4. Shear Stress Transport (SST)

The k–ω based SST model accounts for the transport of turbulent shear stress and gives highly accurate predictions of the onset and amount of flow separation under adverse pressure gradients. The BSL model combines the advantages of Wilcox and k–ε models, but still fails to properly predict the onset and amount of flow separation from smooth surfaces. This results in the overprediction of eddy-viscosity. Proper transport behaviour can be obtained by a limiting to the formulation of eddy-viscosity:

$$v_t = \frac{a_1 k}{\max\left(a_1\omega, SF_2\right)}, \quad (10)$$

where: $v_t = \mu_t/\rho$; F_2 – a blending factor; S – an invariant measure of the strain rate.

3. Simulation of Air Flow around Mine Imitator

A three-dimensional mine imitator model was produced in the *Mechanical Desktop* environment and imported into *ANSYS CFX* program (Fig. 3).

After loading the model of mine imitator, a numerical finite element model is generated in *ANSYS CFX* software. To create a CFX mesh, the type of tetrahedral finite element was chosen. The influence of CFX mesh density on the results was rated by changing the quantity of elements from 0.7 to 1.7 million. Difference in the results under 1.2 and 1.7 million elements was insignificant, and therefore the quantity of 1.2 million elements was used for further calculations. Mine imitator was developed as having a non-slippery but smooth wall. The overall dimensions of mine imitator are 25 mm in diameter and 148 mm in length. The mine was placed inside the channel simulating a wind tunnel. The outside walls of the wind tunnel are modelled as free slip walls. At the inlet, air velocity is set at m/s and at the exit, the precondition is made that air static pressure is constant and equal to 0 Pa. Air temperature is 20° C and reference pressure is 101325 Pa.

Turbulence over mine imitator has been tested applying several turbulence models, including SST, k–ω etc. The obtained results were compared with the experimental ones and presented in the article (Puoti *et al.* 2009). For further research, SST model was selected, since it gave the most accurate comparison with experimental data. The Mach number of overflowing air changed from 0 to 0.7.
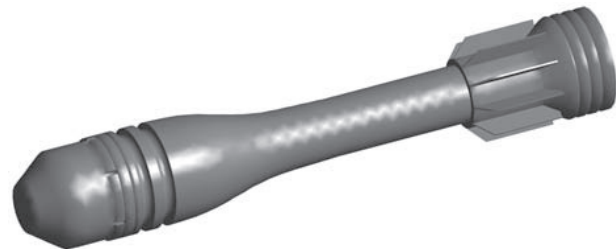

Fig. 3. A model of 25 mm mine imitator

4. Results of Air Flow Simulation

The results of the simulation of air flow around mine imitator were obtained.

Fig. 4 shows the distribution of the force acting on the surface of mine imitator towards X axis. Actual drag force is the sum of drag forces in every mesh node. When the Mach number of air flow is 0.65, actual drag force is 6.11 N.

Full air pressure distribution over mine imitator is shown in Fig. 5 at the Mach number 0.65. The figure shows that the bottom is influenced by the pressure of the opposite direction.

Fig. 6 shows air density distribution when airflow on the surface of the mine at the Mach number is 0.65. Maximum density is received at the front of the mine. The air at the back of the mine thins out.
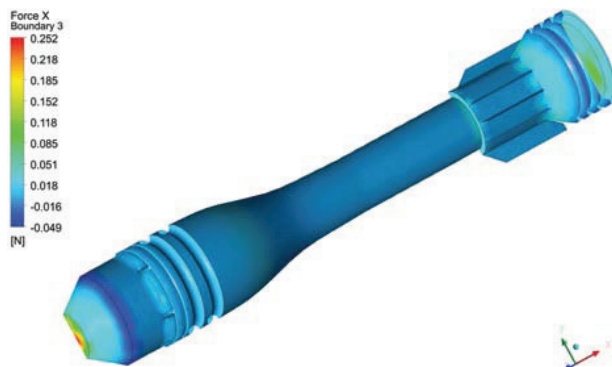
The plot of air flow velocity along X axis is shown in Fig. 7.

Fig. 8 shows velocity streamlines obtained under air flow at the Mach number 0.65.

The drag coefficient of mine imitator was calculated by the following equation (McCormick 1994):

$$C_d = \frac{F_d}{0.5 \cdot \rho \cdot U^2 \cdot A},$$

(11)

where: F_d – drag force obtained from simulation results; ρ – air density at 20 °C; U – mean velocity of air flow, m/s; A – reference area, m^2.

Fig. 9 shows the dependence of the drag force of mine imitator on the Mach number of overflowing air. Together with increasing air speed, force influencing the surface of mine imitator increases. As long as the speed

Fig. 4. Drag force distribution according to X-axis when the Mach number of airflow is 0.65
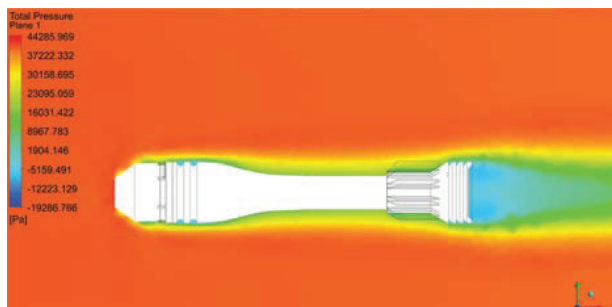

Fig. 5. Full pressure distribution at the moment the air overflows the body when the Mach number of airflow is 0.65
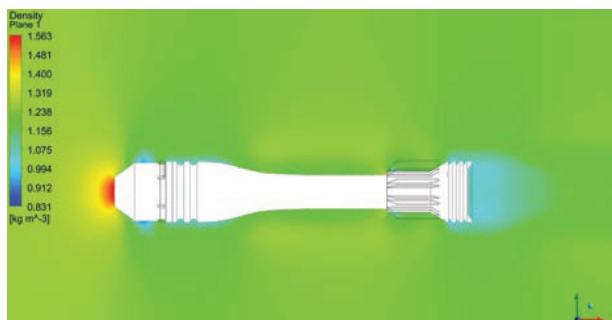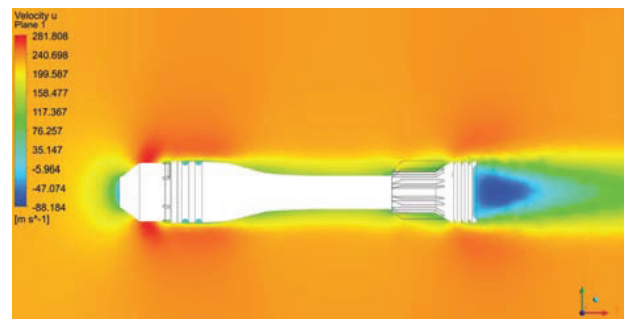

Fig. 6. Air density distribution at the moment the air overflows the body when the Mach number of airflow is 0.65

Fig. 7. The change of airflow speed at the moment the air overflows the body when the Mach number of airflow is 0.65
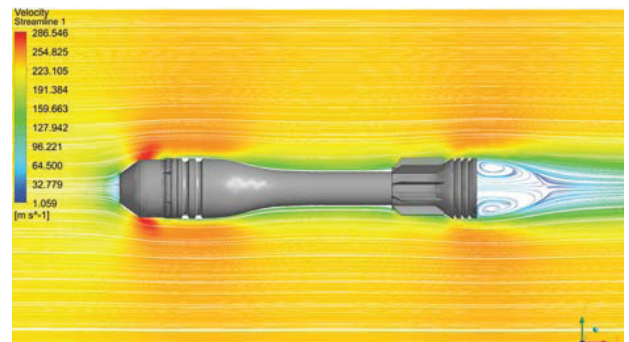

Fig. 8. Velocity streamlines at the moment the air overflows the body when the Mach number of airflow is 0.65
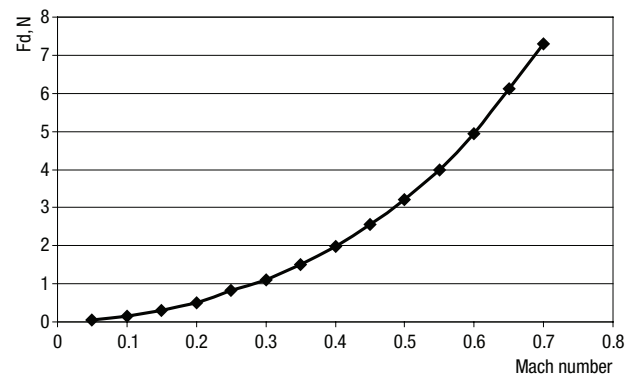

Fig. 9. The dependence of the drag force of the body that is over flown upon the Mach number when air temperature is 20 °C

of the air is not high, force influencing mine imitator is not strong. Along with an increasing speed of overflowing air, drag force non-linearly increases. The drag force values obtained during simulation and the values measured during the experimental study and presented in the article (Puoti *et al.* 2009) differ by no more than 3%.
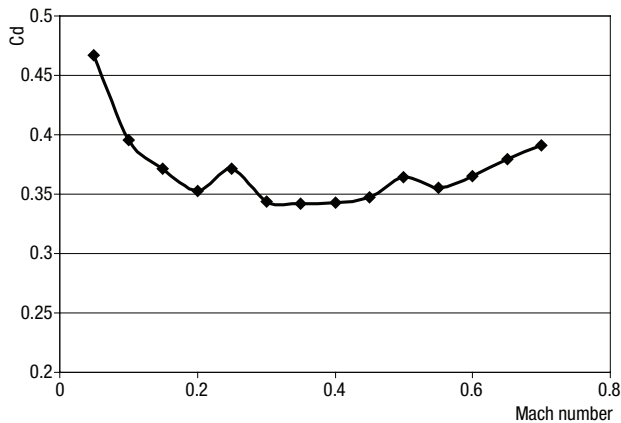

Fig. 10. The dependence of the drag coefficient of the body that is over flown upon the Mach number when air temperature is 20 °C

Fig. 10 shows the dependence of the drag coefficient of mine imitator on the Mach number. While the Mach number is low, makes about 0.05 and is approaching to 0, the drag coefficient is the highest and therefore increases. When friction drag forces prevail, the drag coefficient is the most volatile. When the speed of overflowing air increases, the drag coefficient of the mine imitator reduces, stabilizes and again starts increasing from the Mach number 0.6. When the speed of the mine is about 50 m/s or about Mach 0.15, the drag coefficient of mine imitator will be around 0.37.

5. Conclusions

The goals of this study are to calculate the drag force and drag coefficient of mine imitator. This is the initial investigation that will be continued further. With reference to calculations and their comparison with experimental results, the following conclusions can be made:

1. The model of air flow around mine imitator was created and modelling air overflow around mine imitator was made using *ANSYS CFX* software.
2. After testing several turbulence models, for research purposes, SST turbulence model was chosen, since with the help of this model, the most accurate data was received and compared with experimental models described in the article (Puoti *et al.* 2009).
3. The dependence of the drag force of mine imitator on the speed of overflowing air was calculated. Together with increasing over flowing air speed, force influencing the surface of mine imitator increases. With an increasing speed of overflowing air, drag force non-linearly increases. The drag force values obtained during simulation and the values measured during the

experimental study and presented in the article (Puoti *et al.* 2009) differ by no more than 3%.
4. While the Mach number is low and makes about 0.05, the drag coefficient is the highest and therefore increases. When the speed of overflowing air increases, the drag coefficient of mine imitator reduces, stabilizes and again starts increasing from the Mach number 0.6.

References

ANSYS CFX-Solver Theory Guide. 2006. ANSYS CFX Release 11.0. ANSYS Inc. 312 p.

Fedaravičius, A.; Griškevičius, P.; Jonevičius, V.; Šaulys, P.; Ragulskis, M. K. 2009a. Theoretical basis for creation of mortar firing simulators, in *Mechanika 2009*: *Proceedings of* 14*th International Conference*, 2–3 April 2009. Kaunas, Lithuania, 102–110.

Fedaravičius, A; Šaulys, P; Griskevičius, P. 2009b. Research of mine imitator interaction with deformable surface, *Mechanika* (2): 24–27.

Fedaravičius, A.; Griškevičius, P.; Šaulys, P. 2008a. Interaction modeling of the shell imitator and nondeformable surface, in *Mechanika 2008*: *Proceedings of* 13*th International Conference*, 3–4 April, 2008. Kaunas, Lithuania, 134–138.

Fedaravičius, A.; Šaulys, P.; Griškevičius, P. 2008b. Research of mine imitator interaction with nondeformable surface, *Mechanika* (6): 25–29.

Fedaravičius, A.; Jonevičius, V.; Ragulskis, M. 2007. Development of mortar simulator with shell-in-shell system problem of external ballistics, *Shock and Vibration* 14(5): 371–376.

Fedaravičius, A.; Ragulskis, M.; Klimavičius, Z. 2005. Computational support of the development of a mortar simulator with re-usable shells, *WIT Transactions on Modelling and Simulation: Computational Ballistics II* 40: 381–389.

Fedaravičius, A.; Jonevičius, V.; Ragulskis, M. 2004. Development of mortar training equipment with shell-in-shell system, in *Abstracts: 75th Shock & Vibration Symposium*, 18–22 October, 2004. Virginia Beach, VA, 70–71.

Lee, J. J.; Kang, S. K.; Yoon, S. J.; Park, G. C.; Lee, W. J. 2005. Assessment of turbulence models in CFD code and its application to pebble bed reactor, in 4*th International Conference on Heat Transfer, Fluid Mechanics and Thermodynamics*, 19–22 September 2005. Cairo, Egypt.

McCormick, B. W. 1994. *Aerodynamics, Aeronautics, and Flight Mechanics.* 2nd edition. Wiley. 652 p.

Puoti, V.; Izzo, C.; Valenza, F.; Fedaravičius, A.; Survila, A.; Patašienė, L.; Ragulskis, M. 2009. Experimental Drag Estimation on a Mortar Warhead, in *Transport Means – 2009: Proceedings of* 13*th International Conference*, 22–23 October 2009. Kaunas, Lithuania, 214–216.